arXiv:1409.6095v1 [math.AP] 22 Sep 2014

MAGNETIC RESONANCE-BASED RECONSTRUCTION METHOD OF CONDUCTIVITY AND PERMITTIVITY DISTRIBUTIONS AT THE LARMOR FREQUENCY*

HABIB AMMARI†, HYEUKNAM KWON‡, YOONSEOP LEE‡, KYUNGKEUN KANG§, AND JIN KEUN SEO‡

Abstract. Magnetic resonance electrical property tomography is a recent medical imaging modality for visualizing the electrical tissue properties of the human body using radio-frequency magnetic fields. It uses the fact that in magnetic resonance imaging systems the eddy currents induced by the radio-frequency magnetic fields reflect the conductivity (σ) and permittivity (ϵ) distributions inside the tissues through Maxwell's equations. The corresponding inverse problem consists of reconstructing the admittivity distribution ($\gamma = \sigma + i\omega\epsilon$) at the Larmor frequency ($\omega/2\pi$ =128 MHz for a 3 tesla MRI machine) from the positive circularly polarized component of the magnetic field $\mathbf{H} = (H_x, H_y, H_z)$. Previous methods are usually based on an assumption of local homogeneity ($\nabla\gamma \approx 0$) which simplifies the governing equation. However, previous methods that include the assumption of homogeneity are prone to artifacts in the region where γ varies. Hence, recent work has sought a reconstruction method that does not assume local-homogeneity. This paper presents a new magnetic resonance electrical property tomography reconstruction method which does not require any local homogeneity assumption on γ. We find that γ is a solution of a semi-elliptic partial differential equation with its coefficients depending only on the measured data H^+, which enable us to compute a blurred version of γ. To improve the resolution of the reconstructed image, we developed a new optimization algorithm that minimizes the mismatch between the data and the model data as a highly nonlinear function of γ. Numerical simulations are presented to illustrate the potential of the proposed reconstruction method.

Key words. inverse problems, electrical property tomography, optimal control, conductivity, permittivity, MRI, Maxwell's equations

AMS subject classifications. 35R30, 35J61, 35Q61

1. Introduction.

Magnetic resonance imaging (MRI) system can visualize both the conductivity, σ, and permittivity, ϵ, of biological tissues at the Larmor frequency, which is approximately 128 MHz for a 3 tesla MRI machine. Magnetic resonance electrical property tomography (MREPT) uses a time-harmonic magnetic field inside an imaging object. The standard radio-frequency coil of the magnetic resonance scanner produces the field by feeding in a sinusoidal current at the Larmor frequency. The time-harmonic magnetic field, denoted by $\mathbf{H} = (H_x, H_y, H_z)$, reflects both the conductivity σ and permittivity ϵ of human tissues through the following arrangement of time-harmonic Maxwell's equations:

$$-\Delta\mathbf{H} = \nabla \log(\sigma + i\omega\epsilon) \times [\nabla \times \mathbf{H}] - i\omega\mu_0(\sigma + i\omega\epsilon)\mathbf{H} \qquad \text{in } \Omega, \tag{1.1}$$

where $\mu_0 = 4\pi \times 10^{-7}$ H/m is the magnetic permeability of free space, $\omega/2\pi$ is the Larmor frequency of the MRI scanner, and Ω denotes a three dimensional domain

*This work was supported by the ERC Advanced Grant Project MULTIMOD–267184 and the National Research Foundation of Korea (NRF) grant funded by the Korean government (MEST) (No. 2011-0028868, 2012R1A2A1A03670512).

†Department of Mathematics and Applications, Ecole Normale Supérieure, 45 Rue d'Ulm, 75005 Paris, France (habib.ammari@ens.fr).

‡Department of Computational Science and Engineering, Yonsei University, 50 Yonsei-Ro, Seodaemun-Gu, Seoul 120-749, Korea (3c273-85@hanmail.net, hansubman@naver.com, seoj@yonsei.ac.kr).

§Department of mathematics Yonsei University 50 Yonsei-Ro, Seodaemun-Gu, Seoul 120-749, Korea (kkang@yonsei.ac.kr).

occupying an imaging object. Here, we use the fact that the magnetic permeability of the human body is approximately equal to μ_0.

Clinical MRI scanners measure the positive rotating magnetic field, $H^+ := (H_x + iH_y)/2$, which is the component of the magnetic field $\mathbf{H}$ in the direction $(1, i, 0)/2$. This is because the MR signal, denoted by S, contains partial information about the time-harmonic magnetic field $\mathbf{H} = (H_x, H_y, H_z)$ in the following way

$$S_\tau(\mathbf{r}) \quad \propto \quad M(\mathbf{r})H^-(\mathbf{r})H^+(\mathbf{r})\frac{\sin(\alpha\tau|H^+(\mathbf{r})|)}{|H^+(\mathbf{r})|} \quad \text{for} \quad \mathbf{r} = (x, y, z) \in \Omega, \tag{1.2}$$

where $H^- = (H_x - iH_y)/2$ is the negative rotating magnetic field, $M(\mathbf{r})$ is the standard MR magnitude image at position $\mathbf{r}$, and α is a constant. Here, τ is the duration of the radio-frequency pulse that controls the intensity of the signal S_τ. Acquiring two MR signals S_{τ_1} and S_{τ_2} with suitably chosen τ_1 and τ_2, we can extract the H^+ data through (1.2) with the assumption that $H^+/|H^+| \approx H^-/|H^-|$. This data acquisition technique is called B1 mapping, and was first suggested by Haacke *et al*. [10] in the early nineties. For details on the B1 mapping technique measuring H^+, we refer to numerous published works in the literature [1, 4, 19, 26, 29].

The inverse problem of MREPT consists of reconstructing distributions of σ and ϵ from H^+. To solve the inverse problem, we need to represent the distributions of σ and ϵ with respect to the data H^+. Under the assumption of the local homogeneity, $\nabla(\sigma + i\omega\epsilon) = \mathbf{0}$, the governing partial differential equation (1.1) directly gives the following simple relation between $\sigma + i\omega\epsilon$ and H^+;

$$-\Delta H^+ = -i\omega\mu_0(\sigma + i\omega\epsilon)H^+ \qquad \text{in} \quad \Omega. \tag{1.3}$$

The most widely used MREPT reconstruction methods [30, 12, 13, 14, 15] are based on (1.3) as it gives the direct representation formula for $\sigma + i\omega\epsilon$ with respect to H^+,

$$\sigma + i\omega\epsilon = \frac{1}{i\omega\mu_0}\frac{\Delta H^+}{H^+} \qquad \text{in} \quad \Omega. \tag{1.4}$$

However, when $\nabla(\sigma + i\omega\epsilon)$ is not small, the direct formula (1.4) produces serious reconstruction errors [21]. The local homogeneity assumption neglects the contribution of $\nabla \ln \gamma \times (\nabla \times \mathbf{H})$ in (1.1). Such reconstruction errors are rigorously analyzed in [21].

We need to remove the local homogeneity assumption to develop a reconstruction method. Recently, a reconstruction method [22] removing the assumption of $(\frac{\partial}{\partial x}, \frac{\partial}{\partial y})(\sigma + i\omega\epsilon) = \mathbf{0}$ has been developed, although it still requires the assumption of $\frac{\partial}{\partial z}(\sigma + i\omega\epsilon) = 0$. The method is based on the finding that, under the assumption of longitudinal homogeneity, $\sigma + i\omega\epsilon$ is a solution of a semilinear elliptic PDE with coefficients that only depend on H^+ [22].

In this paper, with no assumption of local homogeneity for $\sigma + i\omega\epsilon$, we develop a new reconstruction method. We find that σ and ϵ satisfy the elliptic partial differential equation,

$$\nabla \cdot \left(G_2[H^+]\nabla \begin{pmatrix} \sigma \\ \epsilon \end{pmatrix} \right) + G_1[\sigma, \epsilon, H^+] \cdot \nabla \begin{pmatrix} \sigma \\ \epsilon \end{pmatrix} + G_0[\sigma, \epsilon, H^+] = 0 \quad \text{in} \quad \Omega, \tag{1.5}$$

where $G_2[H^+]$ is a positive semi-definite matrix, and $G_1[\sigma, \epsilon, H^+]$ and $G_0[\sigma, \epsilon, H^+]$ are vector fields depending only on σ, ϵ, and H^+. Hence, the distribution of σ and ϵ can be

obtained by solving equation (1.5). Unfortunately, $G_2[H^+]$ in (1.5) is degenerate, and thus requires the addition of the weighted diffusion, ρ, to the $(3,3)$ entry of $G_2[H^+]$ so that $G_2[H^+] + \rho \mathbf{e}_3^T \mathbf{e}_3$ is positive definite, where $\mathbf{e}_3 = (0,0,1)$. Thus, (1.5) yields blurred images of σ and ϵ in the z-direction.

To improve the spatial resolution of the reconstructed image, we develop an optimal control method for the parameters σ and ϵ. In the proposed adjoint-based optimization method, the conductivity and permittivity distributions are updated iteratively by a nonlinear optimization algorithm which minimizes the discrepancy function describing the L^2-mismatch between the forward model and the observed data. We compute the Fréchet derivatives of the discrepancy function with respect to σ and ϵ. This optimal control method requires a very good initial guess. Fortunately, we can obtain a good initial guess using (1.5). Several numerical simulations are carried out to show the validity of the proposed reconstruction method.

2. Governing equation for the admittivity reconstruction. We assume that an imaging object occupying a three-dimensional domain Ω with its boundary $\partial\Omega$ being of class $\mathcal{C}^2$. Let $\gamma = \sigma + i\omega\epsilon$ denote the admittivity of the subject at the MR Larmor frequency. For simplicity, we assume that γ is a constant near the boundary; that is, $\gamma = \gamma_0$ in the region $\Omega_d := \{x \in \Omega \mid \mathrm{dist}(x, \partial\Omega) < d\}$ for some $d > 0$, where $\gamma_0 = \sigma_0 + i\omega\epsilon_0$ with σ_0 and ϵ_0 being known reference quantities.

Let $H^s(\Omega)$ denote the standard Sobolev space of order s. We assume that the admittivity distribution $\gamma = \sigma + i\omega\epsilon$ belongs to the following admissible set $\mathcal{A}$:

$$\mathcal{A} = \left\{ \gamma \in H^2(\Omega) \cap L^\infty_{\underline{\lambda},\overline{\lambda}}(\Omega) \mid \omega\mu_0 \|\gamma\|_{H^2} + 8|\Omega|^{1/6} \|\frac{\nabla\gamma}{\gamma}\|_{H^2} < c_1, \;\; \gamma|_{\Omega_d} = \gamma_0 \right\}, \tag{2.1}$$

where $\underline{\lambda}$, $\overline{\lambda}$ and c_1 are positive constants, $|\Omega|$ denotes the volume of Ω, and

$$L^\infty_{\underline{\lambda},\overline{\lambda}}(\Omega) := \left\{ \gamma \in L^\infty(\Omega) : \; \underline{\lambda} < \Re\{\gamma\}, \Im\{\gamma\} < \overline{\lambda} \right\}.$$

The inverse problem is to invert the map $\gamma \to H^+$ where H^+ represents the measured data extracted from the MR signal in (1.2) and the relation between $\mathbf{H}$ and γ is given in (1.1). Noting that the component H_z is known to be relatively small with a regular birdcage coil of MRI scanner [27], we assume $H_z = 0$.

To solve the inverse problem, we need to express $\sigma + i\omega\epsilon$ in terms of H^+ only using the governing equation (1.1). Taking the inner product of both sides of equation (1.1) with the vector $\mathbf{a} = (1, i, 0)/2$, we have

$$-\Delta H^+ = (\nabla \log\gamma \times (\nabla \times \mathbf{H})) \cdot \mathbf{a} - i\omega\mu_0\gamma H^+ \quad \text{in } \Omega. \tag{2.2}$$

It follows from the result of [22] that the contribution of H^- in (2.2) can be eliminated from the identity

$$\begin{aligned}(\nabla \log\gamma \times (\nabla \times \mathbf{H})) \cdot \mathbf{a} \\ = -\nabla \log\gamma \cdot \left(\frac{\partial H^+}{\partial x} - i\frac{\partial H^+}{\partial y}, i\frac{\partial H^+}{\partial x} + \frac{\partial H^+}{\partial y}, \frac{\partial H^+}{\partial z} \right).\end{aligned}$$

Equation (2.2) with the above identity gives the following lemma [22].

LEMMA 2.1. *The γ in (1.1) satisfies the following first-order partial differential equation*

$$\mathcal{L}H^+ \cdot \frac{\nabla\gamma}{\gamma} - i\omega\mu_0\gamma \; H^+ \;\; = \;\; -\Delta H^+ \quad \textit{in } \Omega, \tag{2.3}$$

where $\mathcal{L}$ is the linear differential operator given by

$$\mathcal{L} = \left(-\frac{\partial}{\partial x} + i\frac{\partial}{\partial y}, \quad -i\frac{\partial}{\partial x} - \frac{\partial}{\partial y}, \quad -\frac{\partial}{\partial z} \right). \tag{2.4}$$

According to Lemma 2.1, the inverse problem is reduced to solve the first-order partial differential equation (2.3) for γ. Unfortunately, it may not be possible to solve the first-order partial differential equation (2.3). As the direction vector field of $\mathcal{L}H^+$ is not a real-valued function, the method of characteristics can not be applied. Indeed, Hörmander [11] and Lewy [17] provided non-existence results for the first order partial differential equation with complex-valued coefficients. To be precise, the governing equation (2.3) for H^+ can be rewritten in the standard form $F \cdot \nabla u = f(\cdot, u)$, where $F = \mathcal{L}H^+$, $u = \log \gamma$, and $f(\cdot, u) = i\omega\mu_0 e^u H^+ - \Delta H^+$. According to the Cauchy-Kowalevski theorem [16], the equation $F \cdot \nabla u = f(\cdot, u)$ with suitable initial data, can be locally solvable only when f is analytic. On the other hand, this local solvability can not be guaranteed for general $f \in \mathcal{C}^\infty$ from Lewy's example [17]. This is why we do not use the model (2.3) to compute γ.

2.1. Elliptic equation for the admittivity. In this subsection, we prove that σ and ϵ satisfy the elliptic partial differential equation (1.5) which is one of our main results in this paper. This key observation follows from long and careful computations.

THEOREM 2.2. *The distributions of σ and ϵ satisfy the following equation:*

$$\nabla \cdot \left(A[H^+] \nabla \begin{pmatrix} \sigma \\ \omega\epsilon \end{pmatrix} \right) + F_0[H^+] \cdot \nabla \begin{pmatrix} \sigma \\ \omega\epsilon \end{pmatrix} = \begin{pmatrix} F_1[\sigma, \epsilon, H^+] \\ F_2[\sigma, \epsilon, H^+] \end{pmatrix} \quad in \ \ \Omega, \tag{2.5}$$

where $A[H^+]$ is a positive semi-definite matrix given by

$$A[H^+] = \begin{bmatrix} P_x^2 + P_y^2 & 0 & P_x P_z + P_y Q_z \\ 0 & P_x^2 + P_y^2 & P_y P_z - P_x Q_z \\ P_x P_z + P_y Q_z & P_y P_z - P_x Q_z & P_z^2 + Q_z^2 \end{bmatrix} \quad in \ \ \Omega. \tag{2.6}$$

Here, $F_0[H^+]$, $F_1[\sigma, \epsilon, H^+]$, and $F_2[\sigma, \epsilon, H^+]$ are given by

$$F_0 = -\begin{bmatrix} P_x[H^+]\nabla \cdot P[H^+] + Q_x[H^+]\nabla \cdot Q[H^+] \\ P_y[H^+]\nabla \cdot P[H^+] + Q_y[H^+]\nabla \cdot Q[H^+] \\ P_z[H^+]\nabla \cdot P[H^+] + Q_z[H^+]\nabla \cdot Q[H^+] \end{bmatrix}, \tag{2.7}$$

$$F_1 = -P[H^+] \cdot \nabla\phi[\sigma, \epsilon, H^+] + Q[H^+] \cdot \nabla\psi[\sigma, \epsilon, H^+] + E[\omega\epsilon, H^+], \tag{2.8}$$

$$F_2 = -Q[H^+] \cdot \nabla\phi[\sigma, \epsilon, H^+] - P[H^+] \cdot \nabla\psi[\sigma, \epsilon, H^+] - E[\sigma, H^+], \tag{2.9}$$

where $P[H^+]$, $Q[H^+], E[\eta, H^+]$, $\phi[\sigma, \epsilon, H^+]$ and $\psi[\sigma, \epsilon, H^+]$ are defined by

$$P = (P_x, P_y, P_z) = \left(-\frac{\partial}{\partial x} H_r^+ - \frac{\partial}{\partial y} H_i^+, \ \frac{\partial}{\partial x} H_i^+ - \frac{\partial}{\partial y} H_r^+, \ -\frac{\partial}{\partial z} H_r^+ \right), \tag{2.10}$$

$$Q = (Q_x, Q_y, Q_z) = \left(\frac{\partial}{\partial x} H_i^+ - \frac{\partial}{\partial y} H_r^+, \ \frac{\partial}{\partial x} H_r^+ + \frac{\partial}{\partial y} H_i^+, \ \frac{\partial}{\partial z} H_i^+ \right), \tag{2.11}$$

$$E[\eta, H^+] = Q[H^+] \cdot \nabla(P[H^+] \cdot \nabla\eta) - P[H^+] \cdot \nabla(Q[H^+] \cdot \nabla\eta), \tag{2.12}$$

$$\phi = \omega\mu_0 H_i^+ \sigma^2 - \omega^3 \mu_0 H_i^+ \epsilon^2 + 2\omega^2 \mu_0 H_r^+ \sigma\epsilon + \Delta H_r^+ \sigma - \omega \Delta H_i^+ \epsilon, \tag{2.13}$$

$$\psi = -\omega\mu_0 H_r^+ \sigma^2 + \omega^3 \mu_0 H_r^+ \epsilon^2 + 2\omega^2 \mu_0 H_i^+ \sigma\epsilon + \Delta H_i^+ \sigma + \omega \Delta H_r^+ \epsilon. \tag{2.14}$$

Proof. We first separate the governing equation (2.3) into its real and imaginary parts. Let H_r^+ and H_i^+ be the real and imaginary parts of H^+, i.e., $H^+ = H_r^+ + iH_i^+$. Let γ_i be the imaginary part of the admittivity.

Equation (2.3) can be expressed as

$$-\Delta H^+\gamma = \left(-\frac{\partial H^+}{\partial x} + i\frac{\partial H^+}{\partial y}\right)\frac{\partial \gamma}{\partial x} - \left(i\frac{\partial H^+}{\partial x} + \frac{\partial H^+}{\partial y}\right)\frac{\partial \gamma}{\partial y} - \frac{\partial H^+}{\partial z}\frac{\partial \gamma}{\partial z} - i\omega\mu_0 H^+\gamma^2. \tag{2.15}$$

The real and imaginary parts of equation (2.15) are given, respectively, by

$$\begin{aligned}\Delta H_r^+\sigma - \Delta H_i^+\gamma_i = &\left(\frac{\partial H_r^+}{\partial x} + \frac{\partial H_i^+}{\partial y}\right)\frac{\partial \sigma}{\partial x} - \left(\frac{\partial H_i^+}{\partial x} - \frac{\partial H_r^+}{\partial y}\right)\frac{\partial \gamma_i}{\partial x} \\ &+ \left(\frac{\partial H_r^+}{\partial y} - \frac{\partial H_i^+}{\partial x}\right)\frac{\partial \sigma}{\partial y} - \left(\frac{\partial H_i^+}{\partial y} + \frac{\partial H_r^+}{\partial x}\right)\frac{\partial \gamma_i}{\partial y} \\ &+ \frac{\partial H_r^+}{\partial z}\frac{\partial \sigma}{\partial z} - \frac{\partial H_i^+}{\partial z}\frac{\partial \gamma_i}{\partial z} - \omega\mu_0\left(2H_r^+\sigma\gamma_i + H_i^+(\sigma^2 - \gamma_i^2)\right)\end{aligned} \tag{2.16}$$

and

$$\begin{aligned}\Delta H_r^+\gamma_i + \Delta H_i^+\sigma = &\left(\frac{\partial H_r^+}{\partial x} + \frac{\partial H_i^+}{\partial y}\right)\frac{\partial \gamma_i}{\partial x} + \left(\frac{\partial H_i^+}{\partial x} - \frac{\partial H_r^+}{\partial y}\right)\frac{\partial \sigma}{\partial x} \\ &+ \left(\frac{\partial H_r^+}{\partial y} - \frac{\partial H_i^+}{\partial x}\right)\frac{\partial \gamma_i}{\partial y} + \left(\frac{\partial H_i^+}{\partial y} + \frac{\partial H_r^+}{\partial x}\right)\frac{\partial \sigma}{\partial y} \\ &+ \frac{\partial H_r^+}{\partial z}\frac{\partial \gamma_i}{\partial z} + \frac{\partial H_i^+}{\partial z}\frac{\partial \sigma}{\partial z} + \omega\mu_0\left(H_r^+(\sigma^2 - \gamma_i^2) - 2H_i^+\sigma\gamma_i\right).\end{aligned} \tag{2.17}$$

The real part (2.16) can be written as

$$P[H^+]\cdot\nabla\sigma + Q[H^+]\cdot\nabla\gamma_i + \kappa[\gamma, H^+] = 0 \quad \text{in } \Omega, \tag{2.18}$$

where $\kappa := -\omega\mu_0\left(2H_r^+\sigma\gamma_i + H_i^+(\sigma^2 - \gamma_i^2)\right) - \Delta H_r^+\sigma + \Delta H_i^+\gamma_i$ and P and Q are given in (2.10) and (2.11), respectively. Applying $P[H^+]\cdot\nabla$ and $Q[H^+]\cdot\nabla$ on equation (2.18), we obtain

$$P[H^+]\cdot\nabla(P[H^+]\cdot\nabla\sigma) + P[H^+]\cdot\nabla(Q[H^+]\cdot\nabla\gamma_i) + P[H^+]\cdot\nabla\kappa[\gamma, H^+] \;=\; 0 \tag{2.19}$$

and

$$Q[H^+]\cdot\nabla(P[H^+]\cdot\nabla\sigma) + Q[H^+]\cdot\nabla(Q[H^+]\cdot\nabla\gamma_i) + Q[H^+]\cdot\nabla\kappa[\gamma, H^+] \;=\; 0. \tag{2.20}$$

Similarly, the imaginary part (2.17) can be written as

$$-Q[H^+]\cdot\nabla\sigma + P[H^+]\cdot\nabla\gamma_i + \tau[\gamma, H^+] = 0 \quad \text{in } \Omega \tag{2.21}$$

where $\tau := \omega\mu_0\left(H_r^+(\sigma^2 - \gamma_i^2) - 2H_i^+\sigma\gamma_i\right) - \Delta H_r^+\gamma_i - \Delta H_i^+\sigma$ and P and Q are given in (2.10) and (2.11), respectively. Applying $P[H^+]\cdot\nabla$ and $Q[H^+]\cdot\nabla$ on equation (2.21), we obtain

$$-Q[H^+]\cdot\nabla(Q[H^+]\cdot\nabla\sigma) + Q[H^+]\cdot\nabla(P[H^+]\cdot\nabla\gamma_i) + Q[H^+]\cdot\nabla\tau[\gamma, H^+] \;=\; 0 \tag{2.22}$$

and

$$-P[H^+]\cdot\nabla(Q[H^+]\cdot\nabla\sigma) + P[H^+]\cdot\nabla(P[H^+]\cdot\nabla\gamma_i) + P[H^+]\cdot\nabla\tau[\gamma, H^+] \;=\; 0. \tag{2.23}$$

Subtracting (2.19) from (2.22) yields

$$P[H^+]\cdot\nabla(P[H^+]\cdot\nabla\sigma)+Q[H^+]\cdot\nabla(Q[H^+]\cdot\nabla\sigma)=F_1[\sigma,\epsilon,H^+], \tag{2.24}$$

where F_1 is given in (2.8). Similarly, subtracting (2.20) from (2.23) yields

$$P[H^+]\cdot\nabla(P[H^+]\cdot\nabla\gamma_i)+Q[H^+]\cdot\nabla(Q[H^+]\cdot\nabla\gamma_i)=F_2[\sigma,\epsilon,H^+] \tag{2.25}$$

with F_2 being given by (2.9). A direct computation shows that equation (2.24) can be expressed as

$$\nabla\cdot\left(\left[\begin{array}{ccc} P_x^2+Q_x^2 & P_xP_y+Q_xQ_y & P_xP_z+Q_xQ_z \\ P_xP_y+Q_xQ_y & P_y^2+Q_y^2 & P_xP_z+Q_xQ_z \\ P_xP_z+Q_xQ_z & P_xP_z+Q_xQ_z & P_z^2+Q_z^2 \end{array}\right]\nabla\sigma\right) +F_0[H^+]\cdot\nabla\sigma=F_1[\sigma,\epsilon,H^+]. \tag{2.26}$$

Since $P_x=-Q_y$ and $P_y=Q_x$, $P_xP_y+Q_xQ_y=0$ and therefore, equation (2.26) can be rewritten as

$$\nabla\cdot\big(A[H^+]\nabla\sigma\big)+F_0[H^+]\cdot\nabla\sigma=F_1[\sigma,\epsilon,H^+]\quad\text{in }\ \Omega. \tag{2.27}$$

Similarly, (2.25) gives

$$\nabla\cdot\big(A[H^+]\nabla\epsilon\big)+F_0[H^+]\cdot\nabla\epsilon=F_2[\sigma,\epsilon,H^+]\quad\text{in }\ \Omega. \tag{2.28}$$

Now, it remains to prove that the matrix A is positive semi-definite matrix. A direct computation shows

$$\det(A-\lambda I)=-\lambda\,(\lambda-(P_x^2+P_y^2))\,(\lambda-(P_x^2+P_y^2+P_z^2+Q_z^2)), \tag{2.29}$$

where det denotes the determinant. Hence, all the eigenvalues of the matrix A are non-negative. □

2.2. Approximate solution. Using the elliptic partial differential equation (2.5) in Theorem 2.2, we can compute a fairly good approximation of the true admittivity. Since the matrix A in (2.5) is degenerate, we need a regularization strategy. By adding a regularization term $\rho\mathbf{e}_3^T\mathbf{e}_3$ to the matrix A, we can compute viscosity solution $U^\rho=(\sigma^\rho,\omega\epsilon^\rho)^T$ of the elliptic partial differential equation (2.5):

$$\nabla\cdot\big((A[H^+]+\rho\mathbf{e}_3^T\mathbf{e}_3)\nabla U^\rho\big)+F_0[H^+]\cdot\nabla U^\rho=\left(\begin{array}{c} F_1[U^\rho,H^+] \\ F_2[U^\rho,H^+] \end{array}\right) \tag{2.30}$$

with the Dirichlet boundary condition $U_0=(\sigma_0,\omega\epsilon_0)^T$ on $\partial\Omega$, where $\mathbf{e}_3=(0,0,1)$, superposed T denotes the transpose, and ρ is a small positive constant. Note that the matrix $A+\rho\mathbf{e}_3^T\mathbf{e}_3$ is positive definite, since the eigenvalues of the matrix $A+\rho\mathbf{e}_3^T\mathbf{e}_3$ are

$$\lambda_1=P_x^2+P_y^2$$

$$\lambda_2,\ \lambda_3=\frac{(P_x^2+P_y^2+P_z^2+Q_z^2+\rho)\pm\sqrt{(P_x^2+P_y^2+P_z^2+Q_z^2+\rho)^2-4(P_x^2+P_y^2)\rho}}{2}.$$

By solving equation (2.30), we can get the blurred admittivity image of the true distribution.

3. Adjoint-based optimization method. This section presents adjoint-based optimization method for finding admittivity distribution. A Newton iteration is used to find optimal solution, hence, a fairly good initial guess is required. The approximated solution in section 2.2 is used as an initial guess of the Newton iteration. Let $H_m^+ \in H^1(\Omega)$ be the measured data corresponding to the true admittivity $\gamma^* \in \mathcal{A}$; hence H_m^+ satisfies

$$\mathcal{L}H_m^+ \cdot \frac{\nabla\gamma^*}{\gamma^*} - i\omega\mu_0\gamma^*\ H_m^+ + \Delta H_m^+ = 0 \quad \text{in } \Omega.$$

For $\gamma \in \mathcal{A}$, let $H^+[\gamma]$ be a solution of the Dirichlet problem:

$$\begin{cases} \mathcal{L}H^+[\gamma] \cdot \frac{\nabla\gamma}{\gamma} - i\omega\mu_0\gamma\ H^+[\gamma] + \Delta H^+[\gamma] &= 0 \quad \text{in } \Omega, \\ H^+ &= H_m^+ \quad \text{on } \partial\Omega. \end{cases} \tag{3.1}$$

The equation (3.1) has a unique solution for properly chosen c_1 in the definition of $\mathcal{A}$ in (2.1). From now on, we assume that c_1 is chosen so that (3.1) has a unique solution. Then, the map

$$\gamma \in \mathcal{A} \ \mapsto\ H[\gamma] \tag{3.2}$$

is well-defined.

We define the misfit function $J[\gamma]$ of the variable $\gamma = \sigma + i\omega\epsilon$ by the L^2-norm of the difference between $H^+[\gamma]$ in (3.1) and the measured data H_m^+:

$$J[\gamma] = \frac{1}{2}\int_\Omega |H^+[\gamma] - H_m^+|^2 d\mathbf{r}. \tag{3.3}$$

Since $J[\gamma] = \frac{1}{2}\left\|H^+[\gamma] - H_m^+\right\|^2_{L^2(\Omega)}$, $J[\gamma] \geq 0$ and $J[\gamma]$ has minimum 0 at $H^+[\gamma] = H_m^+$. In this minimization problem, we need to determine the Fréchet derivative of the misfit function J with respect to the control variable γ. Let $\widetilde{\mathcal{A}}$ be defined by

$$\widetilde{\mathcal{A}} = \left\{\delta\gamma \in H^2(\Omega) \cap L^\infty_{\underline{\lambda},\overline{\lambda}}(\Omega) \mid \quad \delta\gamma|_{\Omega_d} = 0\right\}.$$

The following theorem proves the Fréchet differentiability of $H^+[\gamma]$ under the assumption that $c_1 < 1$.

THEOREM 3.1. *Let $c_1 < 1$. For $\gamma \in \mathcal{A}$, the map $\gamma \mapsto H^+$ is Fréchet differentiable. Let $\delta \in \widetilde{\mathcal{A}}$ be such that $\gamma + \delta \in \mathcal{A}$. The Fréchet derivative $DH^+[\gamma](\delta)$ at δ is given by the solution u of the following equation*

$$\begin{cases} \mathcal{L}u \cdot \frac{\nabla\gamma}{\gamma} - i\omega\mu_0\gamma u + \Delta u &= -\left(\mathcal{L}H^+[\gamma] \cdot \nabla\left(\frac{\delta}{\gamma}\right) - i\omega\mu_0\delta H^+[\gamma]\right) \quad \textit{in } \Omega, \\ u &= 0 \quad \textit{on } \partial\Omega. \end{cases} \tag{3.4}$$

Proof. First, remember that for $w \in H^1(\Omega)$,

$$||w||_{L^4(\Omega)} \leq 2|\Omega|^{1/12}||w||_{H^1(\Omega)}. \tag{3.5}$$

Then, defining

$$w_\delta := H^+[\gamma + \delta] - H^+[\gamma] \in H^1(\Omega),$$

it follows from (3.1) that

$$\begin{cases} \mathcal{L}w_\delta \cdot \frac{\nabla(\gamma+\delta)}{\gamma+\delta} - i\omega\mu_0(\gamma+\delta)w_\delta + \Delta w_\delta = \\ \qquad\qquad -\left(\mathcal{L}H^+[\gamma]\cdot\nabla\left(\frac{\delta}{\gamma}\right)\frac{\gamma^2}{\gamma(\gamma+\delta)} - i\omega\mu_0\delta H^+[\gamma]\right) \quad \text{in } \Omega, \\ w_\delta|_{\partial\Omega} = 0. \end{cases} \tag{3.6}$$

Therefore, we have

$$\begin{aligned} \|w_\delta\|_{H^2(\Omega)} \leq \quad & \left\|\mathcal{L}w_\delta \cdot \frac{\nabla(\gamma+\delta)}{\gamma+\delta} - i\omega\mu_0(\gamma+\delta)w_\delta\right\|_{L^2(\Omega)} \\ & + \left\|\mathcal{L}H^+[\gamma]\cdot\nabla\left(\frac{\delta}{\gamma}\right)\frac{\gamma^2}{\gamma(\gamma+\delta)} - i\omega\mu_0\delta H^+[\gamma]\right\|_{L^2(\Omega)}. \end{aligned} \tag{3.7}$$

By Hölder's inequality and Sobolev embedding theorem (see (3.5)), the first term of the right-hand side of (3.7) can be estimated by

$$\left\|\mathcal{L}w_\delta \cdot \frac{\nabla(\gamma+\delta)}{\gamma+\delta} - i\omega\mu_0(\gamma+\delta)w_\delta\right\|_{L^2(\Omega)} \leq c_1 \|w_\delta\|_{H^2(\Omega)}. \tag{3.8}$$

Combining (3.7) and (3.8), we have

$$(1-c_1)\|w_\delta\|_{H^2(\Omega)} \leq \left\|\mathcal{L}H^+[\gamma]\cdot\nabla\left(\frac{\delta}{\gamma}\right)\frac{\gamma^2}{\gamma(\gamma+\delta)} - i\omega\mu_0\delta H^+[\gamma]\right\|_{L^2(\Omega)}. \tag{3.9}$$

By Hölder's inequality and Sobolev embedding theorem, (3.9) can be estimated by

$$\|w_\delta\|_{H^2(\Omega)} \leq C' \|\delta\|_{H^2(\Omega)} \left\|H^+[\gamma]\right\|_{H^2(\Omega)} \tag{3.10}$$

if $c_1 < 1$.

Since the data difference w_δ satisfies (3.6) and u is the solution of equation (3.4), the difference $w_\delta - u \in H^1(\Omega)$ satisfies

$$\begin{aligned} \mathcal{L}(w_\delta-u)\cdot\frac{\nabla\gamma}{\gamma} - i\omega\mu_0\gamma(w_\delta-u) + \Delta(w_\delta-u) \;=\; & -\left(\mathcal{L}w_\delta\cdot\nabla\left(\frac{\delta}{\gamma}\right)\frac{\gamma^2}{\gamma(\gamma+\delta)}\right. \\ & \left. -i\omega\mu_0\delta w_\delta + \mathcal{L}H^+[\gamma]\cdot\nabla\left(\frac{\delta}{\gamma}\right)\frac{\gamma}{\gamma+\delta}\right). \end{aligned} \tag{3.11}$$

From the standard estimation of the Poisson equation, we have

$$\begin{aligned} \|w_\delta-u\|_{H^2(\Omega)} \leq & \left\|\mathcal{L}(w_\delta-u)\cdot\frac{\nabla\gamma}{\gamma} - i\omega\mu_0\gamma(w_\delta-u)\right\|_{L^2(\Omega)} \\ & + \left\|\mathcal{L}w_\delta\cdot\nabla\left(\frac{\delta}{\gamma}\right)\frac{\gamma^2}{\gamma(\gamma+\delta)} - i\omega\mu_0\delta w_\delta + \mathcal{L}H^+[\gamma]\cdot\nabla\left(\frac{\delta}{\gamma}\right)\frac{\gamma}{\gamma+\delta}\right\|_{L^2(\Omega)}. \end{aligned} \tag{3.12}$$

Again, by Hölder's inequality and Sobolev embedding theorem, the first term of the right-hand side of (3.12) can be estimated by

$$\left\|\mathcal{L}(w_\delta-u)\cdot\frac{\nabla\gamma}{\gamma} - i\omega\mu_0\gamma(w_\delta-u)\right\|_{L^2(\Omega)} \leq c_1\|w_\delta-u\|_{H^2(\Omega)}. \tag{3.13}$$

Combining (3.12) and (3.13), we have

$$\begin{aligned} & (1-c_1)\|w_\delta-u\|_{H^2(\Omega)} \leq \\ & \quad \left\|\mathcal{L}w_\delta\cdot\nabla\left(\frac{\delta}{\gamma}\right)\frac{\gamma^2}{\gamma(\gamma+\delta)} - i\omega\mu_0\delta w_\delta + \mathcal{L}H^+[\gamma]\cdot\nabla\left(\frac{\delta}{\gamma}\right)\frac{\gamma}{\gamma+\delta}\right\|_{L^2(\Omega)}. \end{aligned} \tag{3.14}$$

By Hölder's inequality and Sobolev embedding theorem, (3.14) can be estimated by

$$\|w_\delta - u\|_{H^2(\Omega)} \leq C_1 \|\delta\|_{H^2(\Omega)} \|w_\delta\|_{H^2(\Omega)} + C_2 \|\delta\|_{H^2(\Omega)} \left\|H^+[\gamma]\right\|_{H^2(\Omega)} \tag{3.15}$$

if $c_1 < 1$.

By inequalities (3.10) and (3.15), it follows that

$$\|w_\delta - u\|_{H^2(\Omega)} \leq C_1' \|\delta\|^2_{H^2(\Omega)} \left\|H^+[\gamma]\right\|_{H^2(\Omega)} + C_2 \|\delta\|_{H^2(\Omega)} \left\|H^+[\gamma]\right\|_{H^2(\Omega)}. \tag{3.16}$$

Thus,

$$\frac{\|H^+[\gamma+\delta] - H^+[\gamma] - u\|_{H^2(\Omega)}}{\|\delta\|_{H^2(\Omega)}} \to 0 \quad \text{as} \quad \|\delta\|_{H^2(\Omega)} \to 0.$$

Hence, u is the Fréchet derivative of $H^+[\gamma]$ at δ, that is, $DH^+[\gamma](\delta) = u$. □

The following theorem expresses the Fréchet derivative of $J[\gamma]$.

THEOREM 3.2. *For $\gamma = \sigma + i\omega\epsilon \in \mathcal{A}$, the Fréchet derivative of $J[\gamma]$ at $\delta \in \widetilde{\mathcal{A}}$ being such that $\gamma + \delta \in \mathcal{A}$ is given by*

$$DJ[\gamma](\delta) = \Re \int_\Omega \delta \left(\frac{1}{\gamma} \nabla \cdot \left(p \mathcal{L} H^+[\gamma] \right) + i\omega\mu_0 H^+[\gamma] p \right) d\mathbf{r}, \tag{3.17}$$

where p is the solution of the adjoint problem:

$$\begin{cases} \Delta p + \mathcal{L} \cdot \left(p \frac{\nabla\gamma}{\gamma} \right) - i\omega\mu_0\gamma p &= \overline{H^+[\gamma] - H_m^+} & \text{in } \Omega, \\ p &= 0 & \text{on } \partial\Omega. \end{cases} \tag{3.18}$$

Proof. To compute the Fréchet derivative of $J[\gamma]$, we consider the perturbation $J[\gamma+\delta] - J[\gamma]$:

$$\begin{aligned} J[\gamma+\delta] - J[\gamma] &= \frac{1}{2} \int_\Omega \left| H^+[\gamma+\delta] - H_m^+ \right|^2 d\mathbf{r} - \frac{1}{2} \int_\Omega \left| H^+[\gamma] - H_m^+ \right|^2 d\mathbf{r} \\ &= \Re \int_\Omega w_\delta \overline{(H^+[\gamma] - H_m^+)}\, d\mathbf{r} + \frac{1}{2} \int_\Omega w_\delta^2\, d\mathbf{r}, \end{aligned} \tag{3.19}$$

where $w_\delta = H^+[\gamma+\delta] - H^+[\gamma]$. So,

$$\left| J[\gamma+\delta] - J[\gamma] - \Re \int_\Omega w_\delta \overline{(H^+[\gamma] - H_m^+)}\, d\mathbf{r} \right| = \left| \frac{1}{2} \int_\Omega w_\delta^2\, d\mathbf{r} \right|. \tag{3.20}$$

By (3.10),

$$\left| \frac{1}{2} \int_\Omega w_\delta^2\, d\mathbf{r} \right| \;=\; \frac{1}{2} \|w_\delta\|^2_{L^2(\Omega)} \;\leq\; C \|\delta\|^2_{H^2(\Omega)} \left\|H^+[\gamma]\right\|^2_{H^2(\Omega)}.$$

Thus,

$$\lim_{\delta\to 0} \frac{\left| J[\gamma+\delta] - J[\gamma] - \Re \int_\Omega w_\delta \overline{(H^+[\gamma] - H_m^+)}\, d\mathbf{r} \right|}{\|\delta\|_{H^2(\Omega)}} = 0.$$

Therefore, the Fréchet derivative $DJ[\gamma](\delta)$ is $\Re \int_\Omega w_\delta \overline{(H^+[\gamma] - H_m^+)}\ d\mathbf{r}$. Using the adjoint problem (3.18) with the homogeneous Dirichlet boundary condition, we get

$$DJ[\gamma](\delta) = \Re \int_\Omega w_\delta \left(\mathcal{L} \cdot \left(p \frac{\nabla \gamma}{\gamma} \right) - i\omega\mu_0 \gamma p + \Delta p \right)\ d\mathbf{r}.$$

On integrating by parts, it follows that

$$\int_\Omega w_\delta \Delta p\ d\mathbf{r} = \int_{\partial\Omega} w_\delta \frac{\partial p}{\partial \mathbf{n}} ds - \int_\Omega \nabla w_\delta \cdot \nabla p\ d\mathbf{r} = -\int_{\partial\Omega} p \frac{\partial w_\delta}{\partial \mathbf{n}} ds + \int_\Omega p \Delta w_\delta\ d\mathbf{r}.$$

Moreover,

$$\int_\Omega w_\delta\ \mathcal{L} \cdot \left(\frac{\nabla \gamma}{\gamma} p \right) d\mathbf{r} = \int_{\partial\Omega} \mathcal{L} \cdot \left(\frac{\nabla \gamma}{\gamma} p \right) \frac{\partial w_\delta}{\partial \mathbf{n}} ds - \int_\Omega \left(\frac{\nabla \gamma}{\gamma} p \right) \cdot \mathcal{L} w_\delta\ d\mathbf{r}.$$

Hence,

$$DJ[\gamma](\delta) = \Re \int_\Omega p \left(\mathcal{L} w_\delta \cdot \frac{\nabla \gamma}{\gamma} - i\omega\mu_0 \gamma\ w_\delta + \Delta w_\delta \right)\ d\mathbf{r}.$$

Note that w_δ satisfies the following identity:

$$\mathcal{L} w_\delta \cdot \frac{\nabla \gamma}{\gamma} - i\omega\mu_0 \gamma w_\delta + \Delta w_\delta = -\mathcal{L} H^+[\gamma + \delta] \cdot \nabla \left(\frac{\delta}{\gamma} \right) + i\omega\mu_0 \delta H^+[\gamma + \delta]. \quad (3.21)$$

So,

$$DJ[\gamma](\delta) = \Re \int_\Omega p \left(-\mathcal{L} H^+[\gamma] \cdot \nabla \left(\frac{\delta}{\gamma} \right) + i\omega\mu_0 \delta H^+[\gamma] \right) d\mathbf{r}.$$

Since $\mathcal{L} H^+[\gamma] \cdot \nabla \left(\frac{\delta}{\gamma} \right) = \nabla \cdot \left(\frac{\delta}{\gamma} \mathcal{L} H^+[\gamma] \right) - \frac{\delta}{\gamma} (\nabla \cdot \mathcal{L} H^+[\gamma])$,

$$\begin{aligned}
\int_\Omega p \left(-\mathcal{L} H^+[\gamma] \cdot \nabla \left(\frac{\delta}{\gamma} \right) \right) d\mathbf{r} &= -\int_\Omega p\ \nabla \cdot \left(\frac{\delta}{\gamma} \mathcal{L} H^+[\gamma] \right) d\mathbf{r} + \int_\Omega p\ \frac{\delta}{\gamma} (\nabla \cdot \mathcal{L} H^+[\gamma]) d\mathbf{r} \\
&= -\int_{\partial\Omega} p \left(\frac{\delta}{\gamma} \mathcal{L} H^+[\gamma] \right) \cdot \mathbf{n}\ ds + \int_\Omega \nabla p \cdot \left(\frac{\delta}{\gamma} \mathcal{L} H^+[\gamma] \right) d\mathbf{r} \\
&\quad + \int_\Omega p\ \frac{\delta}{\gamma} (\nabla \cdot \mathcal{L} H^+[\gamma]) d\mathbf{r} \\
&= \int_\Omega \frac{\delta}{\gamma} \left(\nabla p \cdot \mathcal{L} H^+[\gamma] + p \nabla \cdot \mathcal{L} H^+[\gamma] \right) d\mathbf{r} \\
&= \int_\Omega \frac{\delta}{\gamma} \nabla \cdot \left(p \mathcal{L} H^+[\gamma] \right) d\mathbf{r}.
\end{aligned}$$

Therefore,

$$DJ[\gamma](\delta) = \Re \int_\Omega \delta \left(\frac{1}{\gamma} \nabla \cdot \left(p \mathcal{L} H^+[\gamma] \right) + i\omega\mu_0 H^+[\gamma] p \right) d\mathbf{r},$$

which completes the proof. □

It is worth mentioning that the smallness assumption on the bound c_1 defined in (2.1) ensures the well-posedness of (3.17) with homogeneous Dirichlet boundary condition.

In the next lemma, we rewrite the adjoint problem (3.18) as a second-order elliptic partial differential equation.

LEMMA 3.3. *For $\gamma = \sigma + i\omega\epsilon$, the adjoint problem (3.18) can be rewritten as*

$$\Delta p + G[\gamma] \cdot \nabla p - (i\omega\mu_0\gamma + \Delta \log \gamma)p = \overline{H^+[\gamma] - H_m^+} \quad \text{in } \Omega \tag{3.22}$$

with the Dirichlet boundary condition $p = 0$ on $\partial\Omega$, where

$$G = -\left(\frac{\partial \log \gamma}{\partial x} + i\frac{\partial \log \gamma}{\partial y}, -i\frac{\partial \log \gamma}{\partial x} + \frac{\partial \log \gamma}{\partial y}, \frac{\partial \log \gamma}{\partial z} \right).$$

Proof. Denote by $v := \log \gamma$. Since the linear operator $\mathcal{L}$ is given by

$$\mathcal{L} = \left(-\frac{\partial}{\partial x} + i\frac{\partial}{\partial y}, -i\frac{\partial}{\partial x} - \frac{\partial}{\partial y}, -\frac{\partial}{\partial z} \right) = -\nabla + i\left(\frac{\partial}{\partial y}, -\frac{\partial}{\partial x}, 0 \right),$$

we obtain

$$\begin{aligned} \mathcal{L} \cdot \left(\frac{\nabla \gamma}{\gamma} p \right) = \mathcal{L} \cdot (p \nabla v) &= -\nabla \cdot (p \nabla v) + i\left(\frac{\partial}{\partial y}, -\frac{\partial}{\partial x}, 0 \right) \cdot (p \nabla v) \\ &= -(p\Delta v + \nabla v \cdot \nabla p) + i\left(\frac{\partial}{\partial y}\left(p\frac{\partial v}{\partial x} \right) - \frac{\partial}{\partial x}\left(p\frac{\partial v}{\partial y} \right) \right) \\ &= -(\Delta v)p + G[\gamma] \cdot \nabla p. \end{aligned} \tag{3.23}$$

Hence, if we substitute (3.23) into the adjoint problem (3.18), we get the second-order elliptic partial differential equation (3.22) and the proof is complete. ∎

4. Newton-type reconstruction algorithm. In the section 3, the Fréchet differentiability of the discrepancy functional J is proven. To find $\gamma \in \mathcal{A}$ such that $J[\gamma] = 0$, we apply the Newton method. The Newton method starts from the linearization of the functional J:

$$J[\gamma + h] \approx J[\gamma] + DJ[\gamma](h), \tag{4.1}$$

where $h \in \widetilde{\mathcal{A}}$ and $\gamma, \gamma + h \in \mathcal{A}$. Let γ_n be the n-th iteration. Given γ_n, Newton's method seeks to find h_n such that

$$J[\gamma_n] + DJ[\gamma_n](h_n) = 0. \tag{4.2}$$

If we update the iteration as $\gamma_{n+1} = \gamma_n + h_n$, $J[\gamma_{n+1}] \approx 0$ by (4.1) and (4.2). Note that $DJ[\gamma](kh) = kDJ[\gamma](h)$ for any real number k by (3.17). The following lemma shows how to find h_n.

LEMMA 4.1. *For given γ_n, $h_n = -\frac{J[\gamma_n]}{DJ[\gamma_n](f_n)} f_n$ satisfies (4.2) for any $f_n \in \widetilde{\mathcal{A}}$ such that $DJ[\gamma_n](f_n) \neq 0$.*

Proof. Note that $J[\gamma_n]$ and $DJ[\gamma_n](f_n)$ are real numbers. So, if we substitute $h_n = -\frac{J[\gamma_n]}{DJ[\gamma_n](f_n)} f_n$ into (4.2), then we obtain

$$J[\gamma_n] + DJ[\gamma_n]\left(-\frac{J[\gamma_n]}{DJ[\gamma_n](f_n)} f_n \right) = J[\gamma_n] - \frac{J[\gamma_n]}{DJ[\gamma_n](f_n)} DJ[\gamma_n](f_n) = 0.$$

Hence, for any $f_n \in \widetilde{\mathcal{A}}$ such that $DJ[\gamma_n](f_n) \neq 0$, $h_n = -\frac{J[\gamma_n]}{DJ[\gamma_n](f_n)} f_n$ is the solution of (4.2). □

Lemma 4.1 proves that we can make the step size h_n of (4.2) if we choose the function $f_n \in \widetilde{\mathcal{A}}$ such that $DJ[\gamma_n](f_n) \neq 0$. Equation (3.17) shows that $DJ[\gamma_n](f_n)$ can be represented by L_2 inner product, $DJ[\gamma_n](f_n) = \Re < f_n, \overline{g_n} >$, where $g_n := \frac{1}{\gamma_n}\nabla \cdot (p_n \mathcal{L} H^+[\gamma_n]) + i\omega\mu_0 H^+[\gamma_n] p_n$. Note that g_n is computed from given γ_n and the solution of the adjoint problem (3.18) p_n. If we choose $f_n = \overline{g_n}$, then $DJ[\gamma_n](f_n) = ||\overline{g_n}||_2^2 = ||g_n||_2^2$. In that case, $DJ[\gamma_n](f_n) \neq 0$ unless $g_n = 0$ and the step size h_n becomes

$$h_n = -\frac{J[\gamma_n]}{DJ[\gamma_n](f_n)} f_n = -\frac{J[\gamma_n]}{||g_n||_2^2}\overline{g_n}.$$

So, the Newton iteration algorithm is given by

$$\gamma_{n+1} = \gamma_n - \frac{J[\gamma_n]}{||g_n||_2^2}\overline{g_n}, \tag{4.3}$$

where $g_n = \frac{1}{\gamma_n}\nabla \cdot (p_n \mathcal{L} H^+[\gamma_n]) + i\omega\mu_0 H^+[\gamma_n] p_n$. It is worth emphasizing that the Newton method guarantees the convergence only when the initial guess γ_0 is close enough to the true solution.

To find a good initial guess for γ, we use an iteration scheme to solve (2.30) with small regularization parameter ρ:

$$\nabla \cdot \left((A[H^+] + \rho \mathbf{e}_3^T \mathbf{e}_3) \nabla U_k^\rho \right) + F_0[H^+] \cdot \nabla U_k^\rho = \begin{pmatrix} F_1[U_{k-1}^\rho, H^+] \\ F_2[U_{k-1}^\rho, H^+] \end{pmatrix}. \tag{4.4}$$

Based on the above iteration scheme, we develop the following reconstruction algorithm.

Step 1. For Given data H^+, compute the matrix $A[H^+]$ in (2.30).

Step 2. From the initial guess $U_0^\rho = (\sigma_0, \omega\epsilon_0)^T$, update the vector $U_k^\rho = (\sigma_k, \omega\epsilon_k)^T$ by solving the semi-elliptic PDE (4.4) with the Dirichlet boundary condition $(\sigma_k, \omega\epsilon_k) = (\sigma^*, \omega\epsilon^*)$ on $\partial\Omega$, where σ^* and ϵ^* are the true values.

Step 3. For a given tolerance ε_1, iterate *Step 2* until $||\gamma^k - \gamma^*|| \leq \varepsilon_1$, where $\gamma^k = \sigma_k + i\omega\epsilon_k$ from $U_k^\rho = (\sigma_k, \omega\epsilon_k)^T$. Result of the iteration $U_k^\rho = (\sigma_k, \omega\epsilon_k)^T$ defines the initial guess $\gamma_0 = \sigma_k + i\omega\epsilon_k$ for the next step.

Step 4. Compute $H^+[\gamma_n]$ from the given γ_n, for $n \geq 0$. From t(3.1), the following equation for H^+ can be obtained:

$$\Delta H^+[\gamma_n] + G[\gamma_n] \cdot \nabla H^+[\gamma_n] - i\omega\mu_0\gamma_n \; H^+[\gamma_n] = 0 \tag{4.5}$$

with $H^+ = H_m^+$ on $\partial\Omega$ and $G[\gamma_n]$ being the vector field in (3.22).

Step 5. Compute the functional $J[\gamma_n] = \frac{1}{2}\int_\Omega |H^+[\gamma_n] - H_m^+|^2 d\mathbf{r}$ and the function g_n given by

$$g_n = \frac{1}{\gamma_n}\nabla \cdot \left(p_n \mathcal{L} H^+[\gamma_n] \right) + i\omega\mu_0 H^+[\gamma_n] p_n \tag{4.6}$$

by solving the following adjoint problem for p_n:

$$\Delta p_n + G[\gamma_n] \cdot \nabla p_n - (i\omega\mu_0\gamma_n + \Delta \log \gamma_n) p_n = \overline{H^+[\gamma_n] - H_m^+} \quad \text{in } \Omega$$

with $p_n = 0$ on $\partial\Omega$.

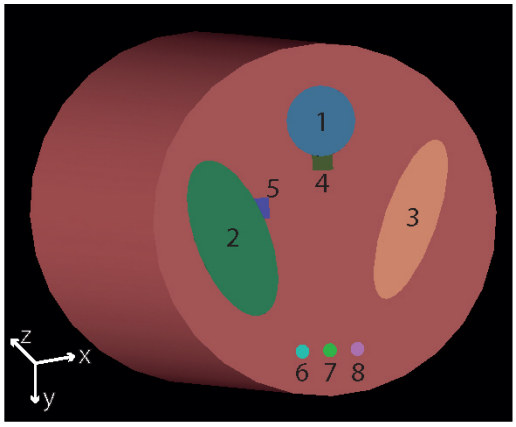

	Conductivity	Relative Permittivity
1	1.5	60
2	1.2	100
3	0.8	50
4	0.7	100
5	0.3	15
6	0.5	30
7	0.2	100
8	1.5	120
Body	1	80

FIG. 5.1. *model configuration (left) and table of the value of electrical property (right).*

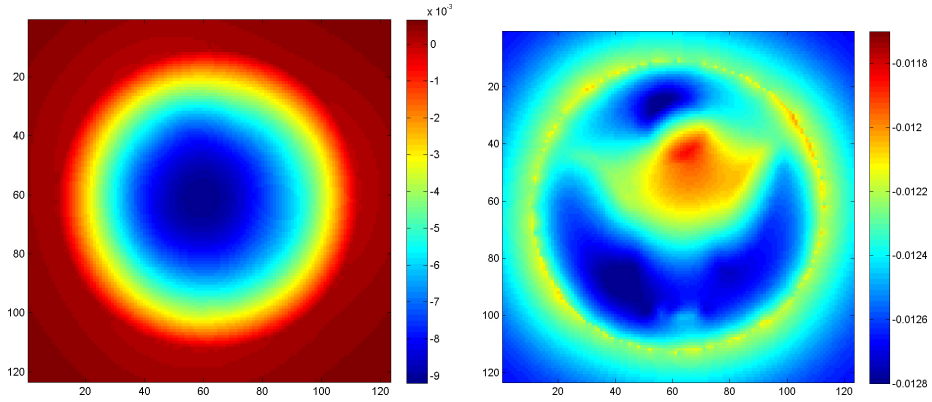

(a) $\Re\left(H^{+}[\gamma^{*}]\right)$ (b) $\Im\left(H^{+}[\gamma^{*}]\right)$

FIG. 5.2. *Real part and imaginary part of the given data in the slice Ω_0; (a) The real part of the data $H^{+}[\gamma^{*}]$, (b) The imaginary part of the data $H^{+}[\gamma^{*}]$.*

Step 6. Update γ_n:

$$\gamma_{n+1} = \gamma_n - \frac{J[\gamma_n]}{||g_n||_2^2}\overline{g_n} \tag{4.7}$$

from $J[\gamma_n]$ and g_n from *Step 5*.

Step 7. For a given tolerance ε_2, repeat from *Step 4* to *Step 6* until $||\gamma_n - \gamma^{*}|| \leq \varepsilon_2$.

5. Numerical simulations. In this section, we will present numerical simulation results from two models to validate the proposed algorithm. In the first model, we set the domain Ω to be a cylindrical model where the admittivity distribution does not change along the z-direction. Figure 5.1 shows the simulation model, the conductivity values σ, and the relative permittivity values $\epsilon/\tilde{\epsilon}$ in the domain, where $\tilde{\epsilon} = 8.85 \times 10^{-12}[F/m]$ is the permittivity of free space. Figure 5.2 shows the real and imaginary parts of the given data, $H^{+}[\gamma^{*}]$ in slice $\Omega_0 = \Omega \cap \{z = 0\}$, where γ^{*} is the true admittivity distribution.

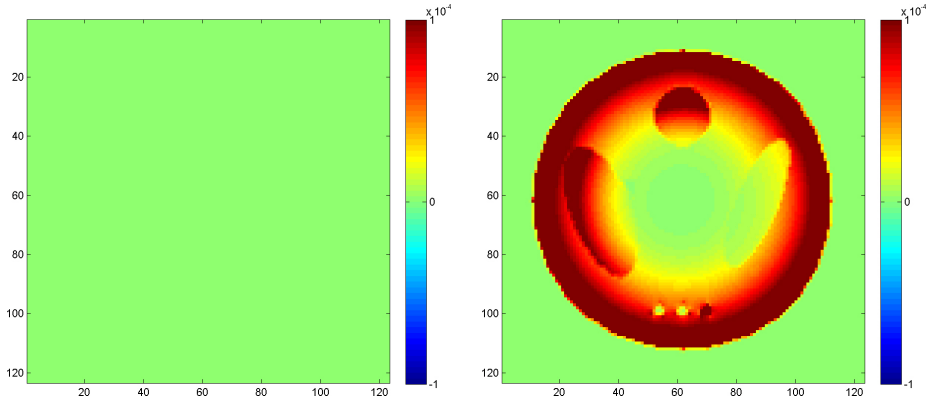

(a) $\det(A[H^+])$ (b) $\det\left(A[H^+] + \rho \mathbf{e}_3^T \mathbf{e}_3\right)$

FIG. 5.3. *(a) Image of the determinant of the matrix $A[H^+]$ in the slice Ω_0. (b) Image of the determinant of the matrix $A[H^+] + \rho \mathbf{e}_3^T \mathbf{e}_3$ in the slice Ω_0, where ρ is 5% of the maximum of A_{33}, $P_z^2 + Q_z^2$ in (2.5).*

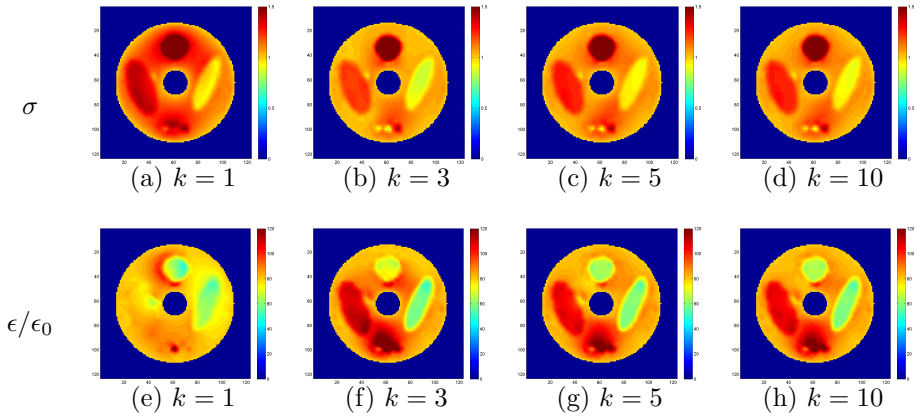

(a) $k = 1$ (b) $k = 3$ (c) $k = 5$ (d) $k = 10$

(e) $k = 1$ (f) $k = 3$ (g) $k = 5$ (h) $k = 10$

FIG. 5.4. *Reconstruction images obtained from the iterative scheme (4.4) with $k = 1, 2, 5, 10$ in the slice Ω_0. (a)-(d): Images of the first row are reconstructed conductivity distribution. (e)-(h): Images of the second row are reconstructed relative permittivity distribution.*

In subsection 2.1, we proved that the solution of (2.5) is the blurred approximation of true admittivity. However, (2.5) is degenerate since the diffusion matrix $A[H^+]$ is singular. So, we modified (2.5) to (4.4) by adding the regularization term $\rho \mathbf{e}_3^T \mathbf{e}_3$. Figure 5.3 shows the determinant of A and $A + \rho \mathbf{e}_3^T \mathbf{e}_3$, where ρ is 5% of the maximum of A_{33}, $P_z^2 + Q_z^2$ in (2.5).

Figure 5.3 explains that the regularized semi-elliptic PDE is also degenerate near $l = \{(0, 0, z) \mid z \in \mathbb{R}\}$. To avoid this, we segmented subdomain D near l, as shown in Figure 5.4. In the subdomain $\Omega \backslash D$, we applied the iteration method (4.4). Figure 5.4 illustrates solutions of (4.4), $U_k = (\sigma_k, \omega\epsilon_k)$, in $\Omega \backslash D$ with various iteration numbers k. We set the initial values to be constant: $\sigma_0 = 1$ and $\omega\epsilon_0 = 0$. In order to check the convergence and the accuracy of the proposed algorithm (4.4), we plotted $||\gamma_k - \gamma^*||_2$ and $||\gamma_k - \gamma_{k-1}||_2$ with $k = 1, 2, \cdots, 10$ in Figure 5.5. Figure 5.5 shows that the iteration method (4.4) converges as k increases and the error between true admittivity and reconstructed admittivity decreases. We choose U_3 to be the solution

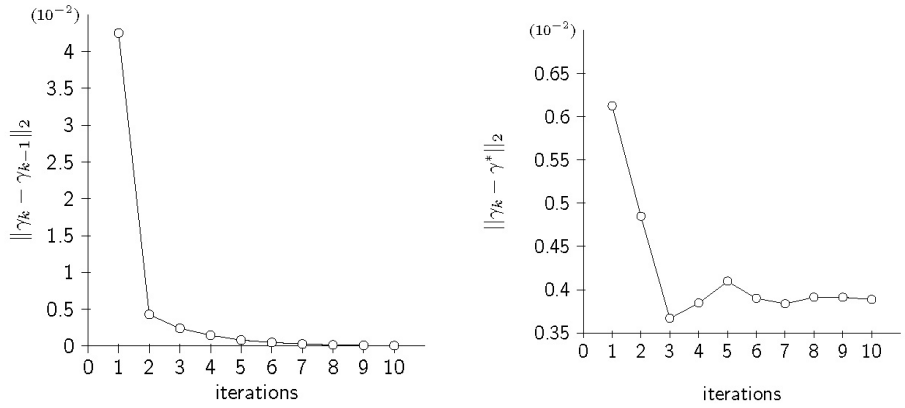

(a) $\|\gamma_k - \gamma_{k-1}\|_2$ (b) $\|\gamma_k - \gamma^*\|_2$

FIG. 5.5. *(a) Plot* $||\gamma_k - \gamma_{k-1}||_2$ *to show the convergence of the iteration (4.4). (b) Plot* $||\gamma_k - \gamma^*||_2$ *to show the accuracy of (4.4) with iteration numbers* $k = 1, 2, \cdots, 10$.

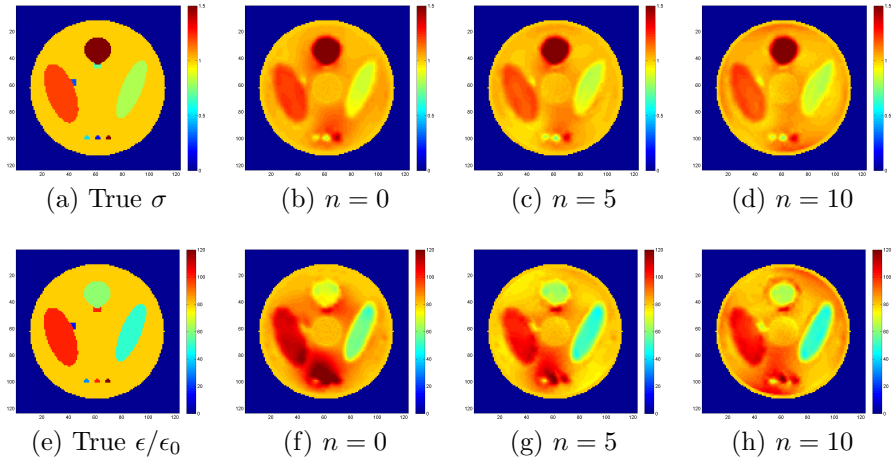

(a) True σ (b) $n = 0$ (c) $n = 5$ (d) $n = 10$

(e) True ϵ/ϵ_0 (f) $n = 0$ (g) $n = 5$ (h) $n = 10$

FIG. 5.6. *Reconstruction images obtained from the Newton method (4.7) with the iteration numbers* $n = 1, 2, 5, 10$, *in the slice* Ω_0. *(a) and (e) are true conductivity and relative permittivity images, respectively. (b), (c) and (d) are the reconstructed conductivity distributions. (f),(g), (h) are the reconstructed relative permittivity distributions.*

of the iterative algorithm. We used direct method (1.4) for the admittivity value γ in the segmented subdomain D. So, we let U_3 with the value obtained from the direct method in D to be the initial guess of the Newton method (4.7). Figure 5.6 illustrates the reconstructed conductivity and relative permittivity distribution by the Newton iteration (4.7). Figure 5.7 shows the functional $J[\gamma_n]$ and the accuracy of the Newton method, $\frac{1}{|S|}\int_S \left|\frac{\gamma_n}{\gamma^*} - 1\right| dx$, where S is the region of anomalres. We defined the accuracy criterion to be $\frac{1}{|S|}\int_S \left|\frac{\gamma_n}{\gamma^*} - 1\right| dx$ in order to see the performance of the Newton method only in the regions containing the anomalies.

To illustrate the performance of the proposed method, we compared the reconstruction results with the true values in Figure 5.8. Figure 5.9 shows the reconstructed

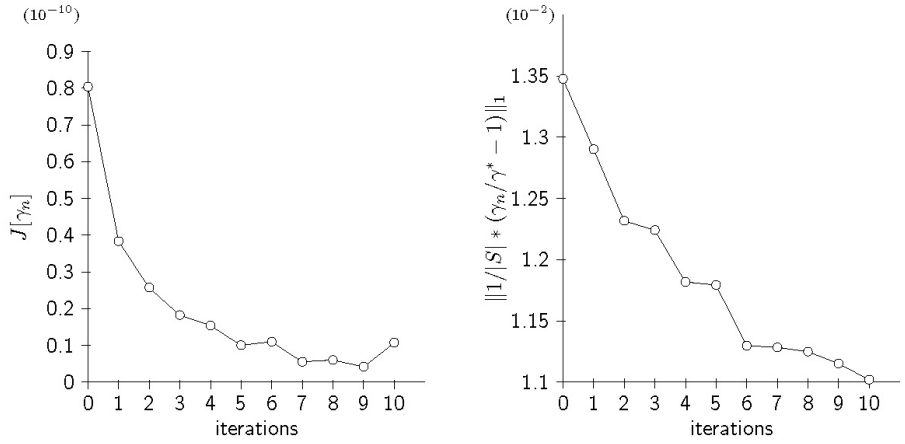

(a) $J[\gamma_n]$ (b) $\frac{1}{|S|}\int_S \left|\frac{\gamma_n}{\gamma^*} - 1\right| dx$

FIG. 5.7. *(a) Plot of the functional $J[\gamma_n]$. (b) Plot of $\frac{1}{|S|}\int_S \left|\frac{\gamma_n}{\gamma^*} - 1\right| dx$ to show the accuracy of (4.4) with the iteration numbers $n = 0, 1, \ldots, 10$.*

images by the direct formula (1.4) and the proposed method. Figure 5.10 compares between the two methods, the direct formula (1.4) and the proposed method, for imaging small anomalies.

In the second numerical model, we simulate the model with admittivity changing along z-direction, i.e., $\frac{\partial \gamma}{\partial z} \neq 0$. The domain Ω is decomposed into two parts, $\Omega_- = \Omega \cap \{z < 0\}$ and $\Omega_+ = \Omega \cap \{z \geq 0\}$. In Ω_-, the admittivity distribution is the same as in Model 1. However, the admittivity distribution in Ω_+ is different from Model 1 and is such that $\frac{\partial \gamma}{\partial z} \neq 0$ in Ω_0. Figure 5.11 shows the second configuration model, the conductivity and the relative permittivity values in the domain. Figure 5.12 shows the reconstruction results using the direct method and the proposed method. Figure 5.13 shows the accuracy of the proposed method applied to the second model. Figure 5.14 presents the reconstructed conductivity distribution of the second model in the slice of Ω_- using the proposed method. Figure 5.13 and Figure 5.14 demonstrate that the proposed method works well in the case of $\frac{\partial \gamma}{\partial z} \neq 0$.

6. Concluding remarks. In this paper, we have developed an iterative novel scheme for reconstructing electrical tissue properties at the Larmor frequency from measurements of the positive rotating magnetic field. We first suggest the elliptic partial differential equation (2.30) which provides a blurred reconstructed image. By considering the blurred reconstructed image as an initial guess of the Newton iteration, the Newton iteration for finding the minimizer of the functional J in (3.3) finds the final reconstruction admittivity. Note that our scheme does not require a local homogeneity assumptions on γ and allows to reconstruct inhomogeneous distributions accurately.

REFERENCES

[1] S. AKOKA, F. FRANCONI, F. SEGUIN, AND A. LE PAPE, *Radiofrequency map of an NMR coil by imaging*, Magn. Reson. Imag., 11 (1993), pp. 437–441.

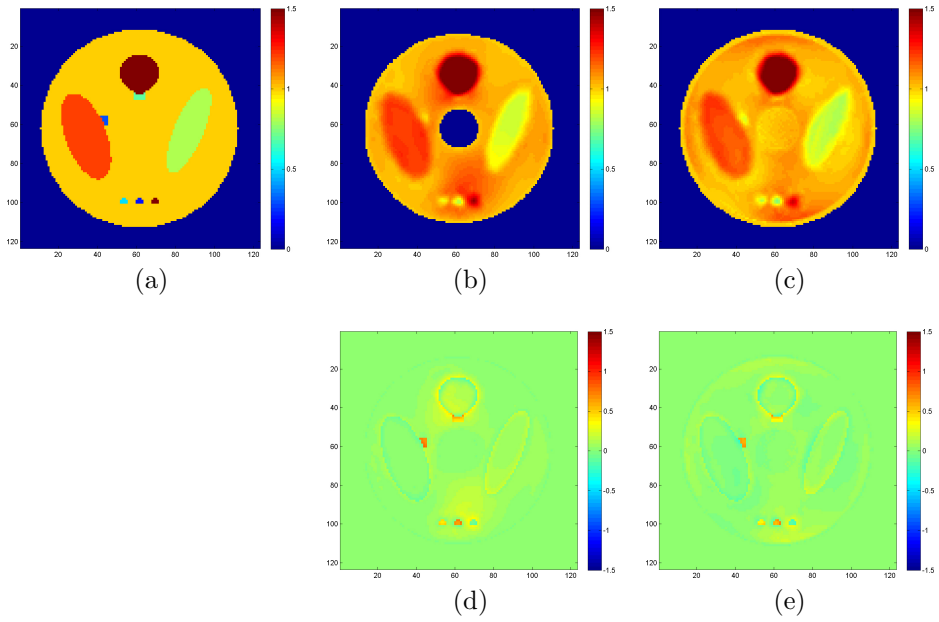

FIG. 5.8. *(a) True conductivity distribution in the slice Ω_0. (b) Reconstructed conductivity image by the semi-elliptic PDE (4.4) with $k = 3$ in the segmented slice $\Omega_0 \backslash D$. (c) Reconstructed conductivity image by the Newton iteration method (4.7) with $n = 10$ in the slice Ω_0. (d) The image of the error of (b) in $\Omega_0 \backslash D$. (e) The image of the error of (c) in Ω_0.*

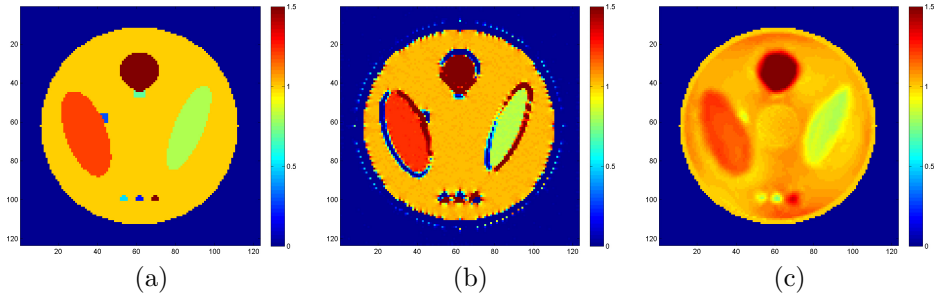

FIG. 5.9. *(a) True conductivity in the slice Ω_0. (b) Reconstructed conductivity obtained from the direct formula (1.4) in Ω_0. (c) Reconstructed conductivity using the proposed method in Ω_0.*

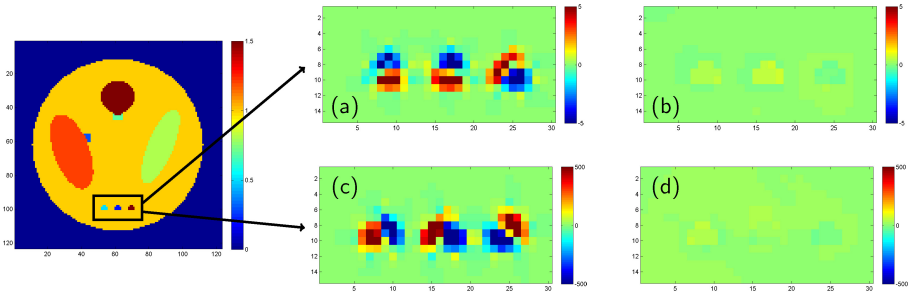

FIG. 5.10. *(a) and (c), respectively, are images of the errors of conductivity and relative permittivity using the direct formula (1.4) in the slice Ω_0. (b) and (d), respectively, are images of the errors of conductivity and relative permittivity using the proposed method in the slice Ω_0.*

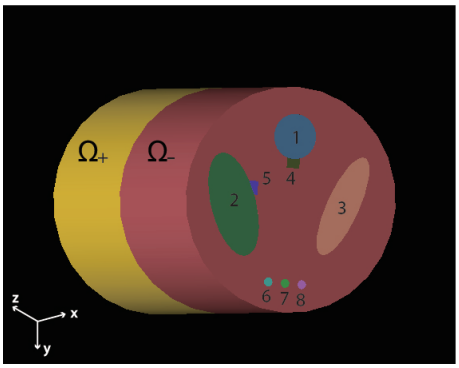

	Conductivity in Ω-, Ω+	Relative Permittivity in Ω-, Ω+
1	1.5, 0.8	60, 100
2	1.2, 0.3	100, 15
3	0.8, 1.5	50, 120
4	0.7, 1.5	100, 80
5	0.3, 1	15, 100
6	0.5, 1	30, 120
7	0.2, 0.5	100, 30
8	1.5, 0.8	120, 80
Body	1, 1.2	80, 60

FIG. 5.11. *Second model configuration (left) and table of the value of electrical property (right).*

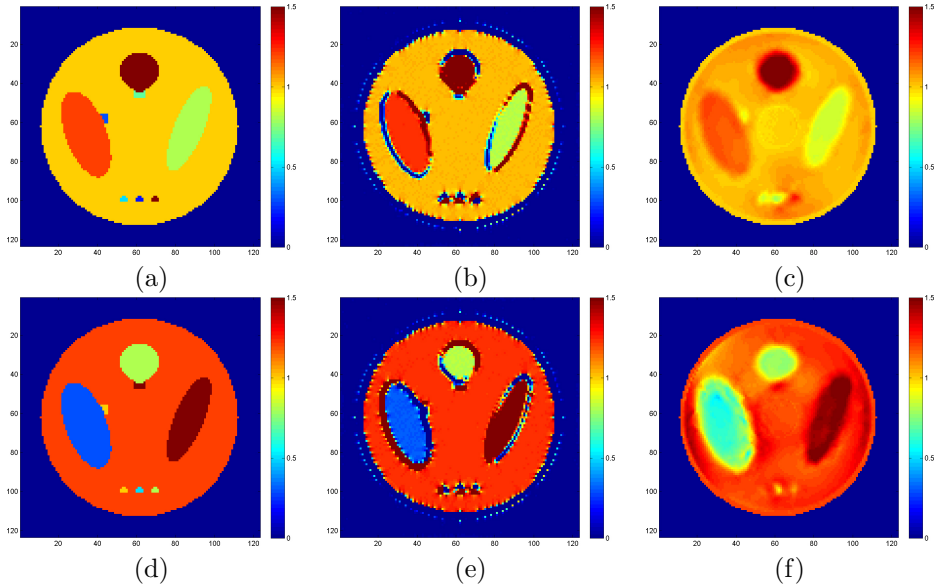

FIG. 5.12. *(a) True conductivity in the slice in Ω_-. (b) Reconstructed conductivity obtained from the direct formula (1.4) in Ω_-. (c) Reconstructed conductivity using the proposed method in Ω_-. (d) True conductivity in the slice in Ω_+. (e) Reconstructed conductivity obtained from the direct formula (1.4) in Ω_+. (f) Reconstructed conductivity using the proposed method in Ω_+.*

[2] H. AMMARI, J. GARNIER, L. GIOVANGIGLI, W. JING, AND J. K. SEO, *Spectroscopic imaging of a dilute cell suspension*, arXiv:1310.1292.

[3] H. AMMARI, L. GIOVANGIGLI, L. NGUYEN, AND J. K. SEO, *Admittivity imaging from multi-frequency micro-electrical impedance tomography* , arXiv:1403.5708.

[4] C. M. COLLINS, Q. X. YANG, J H WANG, X. ZHANG, H. LIU, S. MICHAELI, X.-H. ZHU, G. ADRIANY, J. T. VAUGHAN, P. ANDERSON, H. MERKLE, K. UGURBIL, M. B. SMITH, AND W. CHEN, *Different excitation and reception distributions with a single-loop transmit-receive surface coil near a head-sized spherical phantom at 300 MHz*, Magn. Reson. Med., 47 (2002), pp. 1026–1028.

[5] C. GABRIEL, S. GABRIEL, AND E. CORTHOUT, *The dielectric properties of biological tissues: I. Literature survey*, Phys. Med. Biol., 41 (1996), pp. 2231–2249.

[6] S. GABRIEL, R. W. LAU, AND C. GABRIEL, *The dielectric properties of biological tissues: II.*

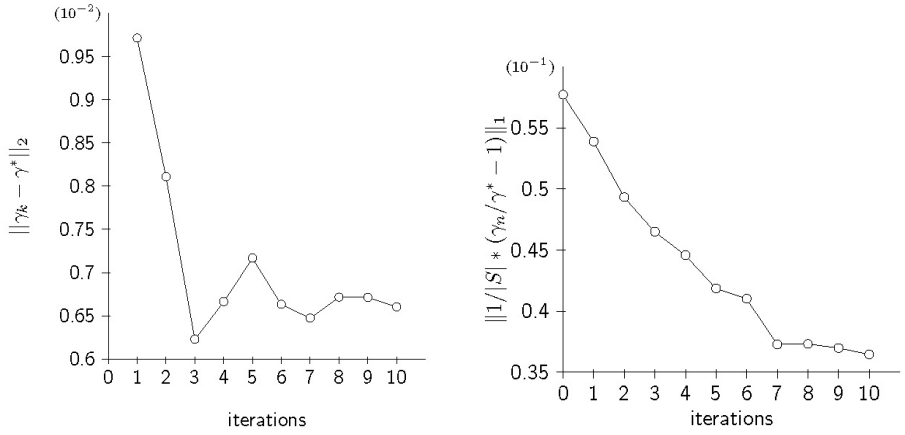

(a) $\|\gamma_k - \gamma^*\|_2$ (b) $\frac{1}{|S|}\int_S \left|\frac{\gamma_n}{\gamma^*} - 1\right| dx$

FIG. 5.13. *(a) Plot of $||\gamma_k - \gamma^*||_2$ to show the accuracy of the semi-elliptic PDE (4.4) with the iteration numbers $k = 1, 2, \cdots, 10$. (b) Plot of $\frac{1}{|S|}\int_S \left|\frac{\gamma_n}{\gamma^*} - 1\right| dx$ to show the accuracy of the Newton iteration (4.4) with the iteration numbers $n = 0, 1, \cdots, 10$.*

Measurements in the frequency range 10 Hz to 20 GHz., Phys. Med. Biol., 41 (1996), pp. 2251–2269.

[7] S. GABRIEL, R. W. LAU, AND C. GABRIEL, *The dielectric properties of biological tissues: III. Parametric models for the dielectric spectrum of tissues*, Phys. Med. Biol., 41 (1996), pp. 2271–2293.

[8] D. GILBARG AND N. S. TRUDINGER, *Elliptic Partial Differential Equations of Second Order*, Classics in Mathematics, Springer-Verlag, Berlin, 2001.

[9] S. GRIMNES AND Ø. G. MARTINSEN, *Bioimpedance and Bioelectricity Basics*, Academic Press, San Diego, 2nd ed., 2008.

[10] E. M. HAACKE, L. S. PETROPOULOS, E. W. NILGES, AND D. H. WU, *Extraction of conductivity and permittivity using magnetic resonance imaging*, Physics in Medicine and Biology, 36 (1991), pp. 723–734.

[11] L. HÖRMANDER, *Linear Partial Differential Operators*, Grundl. Math. Wissenschaft., 116, Springer, 1966.

[12] U. KATSCHER, T. DORNIOK, C. FINDEKLEE, P. VERNICKEL, AND K. NEHRKE, *In vivo determination of electric conductivity and permittivity using a standard MR system*, in 13th International Conference on Electrical Bioimpedance and the 8th Conference on Electrical Impedance Tomography, H. Scharfetter and R. Merwa, eds., vol. 17, Berlin, 2007, Springer-Verlag, pp. 508–511.

[13] U. KATSCHER, M. HANFT, P. VERNICKEL, AND C. FINDEKLEE, *Electric properties tomography (EPT) via MRI*, in Proceedings of the 14th Annual Meeting of ISMRM, Seattle, Washington, USA, vol. 14, 2006, p. 3037.

[14] U. KATSCHER, M. HANFT, P. VERNICKEL, AND C. FINDEKLEE, *Experimental verification of electric properties tomography (EPT)*, in Proc. Intl. Soc. Mag. Reson. Med., vol. 14, 2006, p. 3035.

[15] U. KATSCHER, T. VOIGT, C. FINDEKLEE, P. VERNICKEL, K. NEHRKE, AND O. DOSSEL, *Determination of electric conductivity and local SAR via B1 mapping*, IEEE Trans. Med. Imag., 28 (2009), pp. 1365–1374.

[16] S. VON KOWALEVSKY, *Zur theorie der partiellen differentialgleichung*, J. Reine Angewandte Math., 80 (1875), pp. 1–32.

[17] H. LEWY, *An Example of a smooth linear partial differential equation without solution*, Annals of Math., 66 (1957), pp. 155–158.

[18] S. MIZOHATA, *Solutions nulles et solutions non analytiques*, J. Math. Kyoto Univ. , 1(1962), pp. 271–302.

[19] V. DE MOORTELE, C. AKGUN, G. ADRIANY, S. MOELLER, J. RITTER, C. M. COLLINS, M. B.

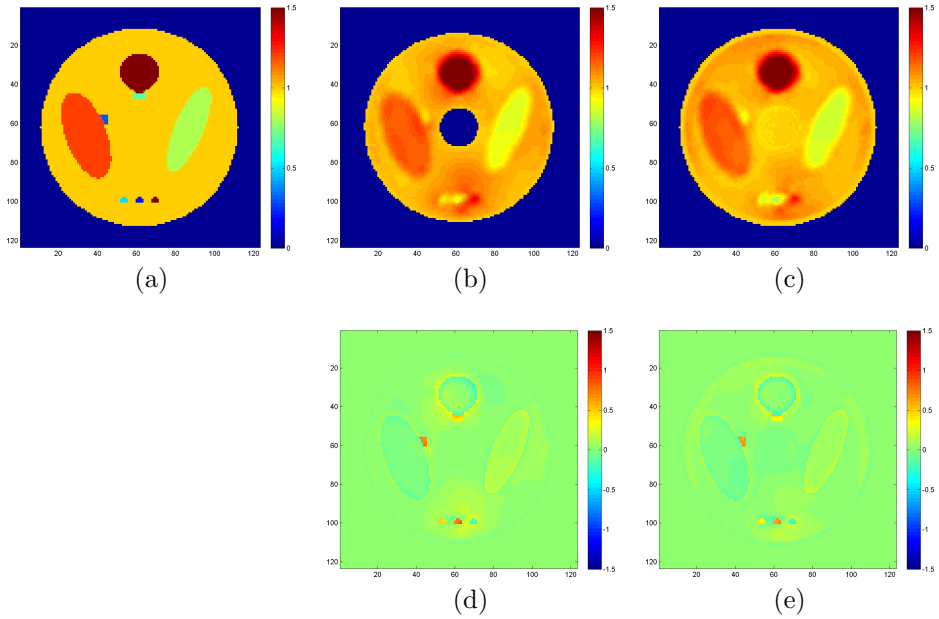

FIG. 5.14. *(a) True conductivity distribution in the slice of Ω_-. (b) Reconstructed conductivity image by the semi-elliptic PDE (4.4) with $k = 3$ in the segmented in the slice of $\Omega_- \backslash D$. (c) Reconstructed conductivity image by the Newton iteration method (4.7) with $n = 10$ in the slice of Ω_-. (d) The image of the error of (b) in the slice of $\Omega_- \backslash D$. (e) The image of the error of (c) in the slice of Ω_-.*

SMITH, J. T. VAUGHAN, K. UGURBIL., *B1 destructive interferences and spatial phase patterns at 7 T with a head transceiver array coil*, Magn. Reson. Med., 54 (2005), pp. 1503–1518.

[20] J. K. SEO, D. H. KIM, J. LEE, O. I. KWON, S. Z. K. SAJIB, AND E. J. WOO, *Electrical tissue property imaging using MRI at dc and Larmor frequency*, Inverse Problems, 28 (2012), 084002, 26pp.

[21] J. K. SEO, M. O. KIM, J. LEE, N. CHOI, E. J. WOO, H. J. KIM, O. I. KWON, AND D. H. KIM, *Error analysis of nonconstant admittivity for MR-based electric property imaging*, IEEE Trans. Med. Imag., 31 (2012), pp. 430–437.

[22] Y. SONG AND J. K. SEO, *Conductivity and permittivity image reconstruction at the Larmor frequency using MRI*, SIAM J. Appl. Math., 73 (2013), pp. 2262–2280.

[23] J. K. SEO AND E. J. WOO, *Magnetic resonance electrical impedance tomography (MREIT)*, SIAM Rev., 53 (2011), pp. 40–68.

[24] J. K. SEO, J. R. YOON, E. J. WOO, AND O. KWON, *Reconstruction of conductivity and current density images using only one component of magnetic field measurements*, IEEE Trans. Biomed. Eng., 50 (2003), pp. 1121–1124.

[25] J. K. SEO, E. J. WOO, U. KATSCHER, AND Y. WANG, *Electro-Magnetic Tissue Properties MRI*, Imperial College Press, Singapoor, 2014.

[26] R. STOLLBERGER AND P. WACH, *Imaging of the active B1 field in vivo*, Magn. Reson. Med., 35 (2005), pp. 246–251.

[27] J. T. VAUGHAN, G. ADRIANY, C. J. SNYDER, J. TIAN, T. THIEL, L. BOLINGER, H. LIU, L. DELABARRE, AND K. UGURBIL, *Efficient high-frequency body coil for high-field MRI*, Magn. Reson. Med., 52 (2004), pp. 851–859.

[28] T. VOIGT, U. KATSCHER, AND O. DOESSEL, *Quantitative conductivity and permittivity imaging of the human brain using electric properties tomography*, Magn. Reson. Med., 66 (2011), pp. 456–466.

[29] J. WANG, M. QIU, Q. X. YANG, M. B. SMITH, AND R. T. CONSTABLE, *Measurement and correction of transmitter and receiver induced nonuniformities in vivo*, Magn. Reson. Med., 53 (2005), pp. 408–417.

[30] H. WEN, *Noninvasive quantitative mapping of conductivity and dielectric distributions using*

RF wave propagation effects in high-field MRI, in Proceedings of SPIE, M. J. Yaffe and L. E. Antonuk, eds., vol. 5030, San Diego, CA, 2003, pp. 471–477.

[31] E. J. Woo and J. K. Seo, *Magnetic resonance electrical impedance tomography (MREIT) for high-resolution conductivity imaging*, Physiol. Meas., 29 (2008), pp. R1–R26.